Proteomics identifies a type I IFN, prothrombotic hyperinflammatory circulating COVID-19 neutrophil signature distinct from non-COVID-19 ARDS

Leila Reyes[1†], Manuel A. Sanchez-Garcia[1†], Tyler Morrison[1†], Andrew J.M. Howden[2†], Emily R. Watts[1], Simone Arienti[1], Pranvera Sadiku[1], Patricia Coelho[1], Ananda S Mirchandani[1], David Hope[3], Sarah K. Clark[3], Jo Singleton[3], Shonna Johnston[1], Robert Grecian[1], Azin Poon[1], Sarah Mcnamara[1], Isla Harper[1], Max Head Fourman[3], Alejandro J. Brenes[2,4], Shalini Pathak[2], Amy Lloyd[2], Gio Rodriguez Blanco[5], Alex von Kriegsheim[5], Bart Ghesquiere[6], Wesley Vermaelen[6], Camila T. Cologna[6], Kevin Dhaliwal[1], Nik Hirani[1], David Dockrell[1], Moira K. Whyte[1], David Griffith[3], Doreen A. Cantrell[2], Sarah R. Walmsley[1*]

[1]University of Edinburgh Centre for Inflammation Research, Queen's Medical Research Institute, University of Edinburgh, Edinburgh, UK.

[2]Division of Cell Signalling and Immunology, University of Dundee, Dundee, UK.

[3]Anaesthesia, Critical Care and Pain, University of Edinburgh, Royal Infirmary of Edinburgh, Edinburgh UK.

[4]Centre for Gene Regulation and Expression, University of Dundee, Dundee, UK.

[5]The University of Edinburgh MRC Institute of Genetics and Molecular Medicine, University of Edinburgh, Edinburgh, UK.

[6]Laboratory of Angiogenesis and Vascular Metabolism, Vesalius Research Centre, Leuven, Belgium.

[†]Contributed equally to the work

*Corresponding author. Email: sarah.walmsley@ed.ac.uk

Summary

Understanding the mechanisms by which infection with SARS-CoV-2 leads to acute respiratory distress syndrome (ARDS) is of significant clinical interest given the mortality associated with severe and critical coronavirus induced disease 2019 (COVID-19). Neutrophils play a key role in the lung injury characteristic of non-COVID-19 ARDS, but a relative paucity of these cells is observed at post-mortem in lung tissue of patients who succumb to infection with SARS-CoV-2. With emerging evidence of a dysregulated innate immune response in COVID-19, we undertook a functional proteomic survey of circulating neutrophil populations, comparing patients with COVID-19 ARDS, non-COVID-19 ARDS, moderate COVID-19, and healthy controls. We observe that expansion of the circulating neutrophil compartment and the presence of activated low and normal density mature and immature neutrophil populations occurs in both COVID-19 and non-COVID-19 ARDS. In contrast, release of neutrophil granule proteins, neutrophil activation of the clotting cascade and formation of neutrophil platelet aggregates is significantly increased in COVID-19 ARDS. Importantly, activation of components of the neutrophil type I IFN responses is specific to infection with SARS-CoV-2 and linked to metabolic rewiring. Together this work highlights how differential activation of circulating neutrophil populations may contribute to the pathogenesis of ARDS, identifying processes that are specific to COVID-19 ARDS.

Keywords

Neutrophil, SARS-CoV-2, COVID-19, ARDS, Type I IFN, platelets

Introduction

Coronavirus disease (COVID-19) is an acute respiratory condition caused by novel coronavirus (SARS-CoV-2, also known as 2019-nCoV) infection. In the most severe cases (termed "Critical COVID-19"), infection with SARS-CoV-2 can lead to the development of acute respiratory distress syndrome (ARDS) (Huang et al., 2020). ARDS is a clinical syndrome defined by the presence of bilateral pulmonary infiltrates on chest radiograph and arterial hypoxaemia that develops acutely in response to a known or suspected insult. Prior to the emergence of SARS-CoV-2, ARDS was known to be the consequence of disordered inflammation (ARDS Network, 2000), and is characterised by a protein-rich oedema in the alveoli and lung interstitium, driven by epithelial and vascular injury (ARDS Network, 2000; Dreyfuss and Saumon, 1993) and increased vascular permeability (Bachofen and Weibel, 1977; Flick et al., 1981). Limited data exists regarding the mechanisms causing hypoxaemia and lung inflammation following infection with SARS-CoV-2, although post-mortem case reports provide evidence of diffuse alveolar damage, with the presence of proteinaceous exudates in the alveolar spaces, intra-alveolar fibrin and alveolar wall expansion (Tian et al., 2020). In previously described ARDS cohorts in which SARS-CoV-2 was not an aetiological factor, alveolar damage is associated with worsening hypoxia and increased mortality. In this context, hypoxia is a key driver of dysfunctional inflammation in the lung, augmenting neutrophil survival (Eltzschig and Carmeliet, 2011; Walmsley et al., 2005) and promoting the release of pro-inflammatory mediators including neutrophil elastase that cause ongoing tissue injury (ARDS Network, 2000; Dreyfuss and Saumon, 1993). Non-dyspnoeic hypoxia is widely described in patients with severe COVID-19 (Tobin, 2020), where it is associated with altered circulating leukocyte profiles with an increase in neutrophil to lymphocyte ratios and the presence of lymphopaenia (Liu et al., 2020; Zhao et al., 2020). More recently, post-mortem studies have revealed that the diffuse alveolar damage does not directly associate with the

detection of virus, supporting the concept of aberrant host immune responses as drivers of tissue injury and pulmonary disease progression (Dorward et al., 2020). A disordered myeloid response is further supported by analysis of gene clusters and surface protein expression of whole blood and peripheral blood mononuclear cell (PBMC) layers of patients with mild and severe COVID-19, identifying a suppressive myeloid cell response in severe disease (Schulte-Schrepping et al., 2020). Whether these populations are specific to COVID-19 ARDS, or also observed in non-COVID-19 ARDS remains to be explored, as does the functional importance of these transcriptional signatures. Finally, the paucity of neutrophil signatures at post-mortem within the lung interstitium and airspaces, together with evidence for increased myelopoesis, raises the important question as to whether neutrophils are being activated and retained within, thus contributing to vascular injury and thrombosis, and highlights important and currently un-explored differences between the pathogenesis of COVID-19 and non-COVID-19 ARDS.

In this program of work, we compared the blood neutrophil populations of patients with COVID-19 ARDS to those of patients with non-COVID-19 ARDS, moderate COVID-19 and healthy controls to define the neutrophil host response to SARS-CoV-2. We reveal that patients with ARDS with or without SARS-CoV-2 infection have an expansion of the circulating neutrophil compartment and identify the presence of activated low and normal density mature and immature neutrophil populations. Analysis of more than 3000 proteins from each of these neutrophil populations characterises the dynamic changes in the neutrophil proteome that are common to COVID-19 and non-COVID-19 ARDS, those that are enriched in COVID-19 ARDS and those that are specific to infection with SARS-CoV-2. Whilst normal density neutrophil (NDN) populations in ARDS demonstrate activation in the circulation irrespective of the cause, release of neutrophil granule proteins and formation of neutrophil platelet aggregates with activation of the clotting cascade is significantly increased in COVID-

19 ARDS and predominantly observed in the low-density mature neutrophil population. Importantly, activation of the type I interferon (IFN) signalling pathways dominates the COVID-19-specific signature, reprogramming neutrophil metabolism and paralleled with up-regulation of proteins required for MHC class I antigen presentation, which are relevant for the innate anti-viral response.

Results

Study population cohorts

To define the circulating neutrophil response to infection with SARS-CoV-2 we studied peripheral blood neutrophil populations isolated from hospitalised patients with moderate COVID-19 and COVID-19 ARDS, comparing these to critical care patients with non-COVID-19 ARDS and healthy controls (Figure 1A). Patient demographic details are provided in Table S1. The presence of ARDS was defined using the Berlin criteria (ARDS Task Force, 2012), and infection with SARS-CoV-2 confirmed either on nasopharyngeal swab, or deep airway samples. In accordance with the WHO COVID-19 classification, patients recruited had either moderate (clinical signs of pneumonia with oxygen saturations >90%) or critical (ARDS) COVID-19 (WHO, 2020).

Circulating neutrophil populations are expanded in COVID-19 and non-COVID-19 ARDS

To explore the different neutrophil populations, flow cytometry analysis of whole blood was first performed to identify CD66b+ cells as neutrophils, with CD16 used as a marker of maturity. CD66b+CD16+ and CD66b+CD16- cells were observed, indicating the presence of a heterogenous population of mature and immature neutrophils in ARDS patients, regardless of COVID-19 status (Figure 1B). Given immature neutrophils are characteristically low-

density neutrophils (LDN) and associated with disease (Silvestre-Roig et al., 2019), flow cytometry analysis was performed on polymorphonuclear (PMN) and peripheral blood mononuclear cell (PBMC) layers isolated using Percoll density gradients. Further characterisation of neutrophil maturity was undertaken by CD10 expression and showed both a mature (CD66b+CD16+CD10+) and immature (CD66b+CD16-CD10-) LDN population in the PBMC layer of non-COVID-19 and COVID-19 ARDS patients (Figure 1C). In contrast, these populations are notably absent in the PBMC layer of healthy control individuals (Figure 1C). Importantly, these LDN populations demonstrated evidence of increased activation states with loss of CD62L (Figure 1D), and upregulation of both CD66b and CD63 (Figure 1E-F). Total neutrophil counts generated from Percoll preparations showed a large expansion of neutrophils in ARDS (Figure 1G). Though a major proportion of the neutrophil population consisted of mature NDN from the PMN layer, there was an increase in the proportion of LDN CD66b+CD16-CD10- in ARDS, which was exacerbated in ARDS patients with COVID-19 (Figure 1H).

Circulating neutrophils restructure their proteomes with up regulation of pro-inflammatory processes common to both COVID-19 and non-COVID-19 ARDS

To understand changes in the functional proteome of circulating neutrophils we used label free Data Independent Acquisition (DIA) mass spectrometry approach. Estimates of protein copy numbers per cell were calculated using the histone ruler method (Wisniewski et al., 2014), along with total cellular protein content and the mass of subcellular compartments. We compared protein abundance between non-COVID-19 ARDS, COVID-19 ARDS and healthy control neutrophil populations. Analysis of the NDN populations common to both healthy control and ARDS identified nearly 5000 proteins (Figure 2A), with a subtle reduction in the total protein content of COVID-19 ARDS neutrophils (Figure 2B). We observed preservation

of global cellular processes across all disease groups evidenced by equivalent mitochondrial protein content (Figure 2C), ribosomal protein content (Figure 2D), and nuclear envelope protein abundance (Figure 2E). Cytoskeletal protein abundance was modestly reduced which may contribute towards the subtle reduction in the total protein content of COVID-19 ARDS neutrophils (Figure 2F). Key components of the translation initiation complex were conserved across health and disease groups (Figure 2G). This would suggest that any differences observed in key neutrophil functions are not driven by a loss of core cellular processes and, therefore, more likely to be consequent upon activation of signalling pathways in response to infectious and inflammatory challenges. Whilst globally there was little to no evidence of changes in protein abundance that would alter transcription factor activity, in keeping with the engagement of innate immune responses following infection with SARS-CoV-2, COVID-19 ARDS neutrophils did regulate expression of the type I IFN regulated proteins Tripartite Motif Containing 22 (TRIM22) and Interferon Regulatory Factor 3 (IRF3) to a greater degree than ARDS alone (Figure 2H).

To determine which components of the neutrophil proteome remodel in patients with COVID-19 and non-COVID-19 ARDS we undertook Linear Models for Microarray data (LIMMA) analysis to identify significant differences in protein abundance (Data S1). We identified almost 200 proteins to be increased in abundance between ARDS (all cause) and healthy control neutrophils (Figure 3A). Gene ontology (GO) term enrichment analysis of these differentially regulated proteins identified a COVID-19 signature which was defined by a greater abundance of proteins in the platelet degranulation and type I IFN signalling pathways (Figure 3B). Immune responses classified by the expression of C-C motif chemokine receptor 1 (CCR1), interleukin 1 receptor Type 2 (IL-1R2), Interleukin 18 receptor 1 (IL-18R1), Interleukin 2 receptor subunit gamma (IL2RG) and TRIM22 were common to both COVID-

19 and non-COVID-19 ARDS, whilst expression of chloride and bicarbonate transporters comprised the ARDS (non-COVID-19) signature (Figure 3B). Around 150 proteins were found at reduced abundance in ARDS (all cause) versus healthy control neutrophils including some proteins that were specific to COVID-19 (Data S1). However, distinct pathways impacted by SARS-CoV-2 infection were not identified among those proteins with reduced abundance.

COVID-19 ARDS neutrophils form aggregates with platelets and activate prothrombotic pathways with enrichment in the low density population

A striking clinical and post-mortem observation in patients with COVID-19 is the prevalence of micro and macrovascular thrombosis. Together with our identification of a platelet degranulation signature within the COVID-19 ARDS samples, this led us to question whether neutrophils could be contributing to an immune mediated thrombosis in COVID-19. Both NDN and LDN displayed an overall increase in proteins associated with fibrin clot formation; fibrinogen alpha, fibrinogen beta and factor XIII (Figure 4A-C) and a failure to induce proteins that inhibit fibrin clot formation in NDN (Figure 4D). This signature was greatest in COVID-19 ARDS neutrophils and enriched within the LDN populations (Figure 4A-C). Importantly, we also detected a clear platelet protein signature with the presence of the platelet proteins platelet factor 4, platelet basic protein and P-selectin (Figure 4E-G) in keeping with the formation of neutrophil platelet aggregates. Confocal imaging on sorted LDN from COVID-19 ARDS patients subsequently revealed the existence of a direct physical association between LDN and platelets in these patients, as opposed to neutrophils from healthy donors (Figure 4H). To understand how neutrophil platelet aggregates were forming we looked for evidence of platelet activation on the neutrophil surface, and neutrophil expression of adhesion molecules involved in platelet interactions. Initial measurements for expression of CD41, a marker of platelet activation, revealed the presence of CD41 on mature LDN isolated from

COVID-19 patients (Figure 4I). This coincided with a significant increase in mature LDN expression of the CD11b component of the Mac-1 platelet binding complex, and a modest uplift in CD18 (Figure 4J). This phenotype was specific to the mature low density population, with only low-level surface expression of CD41, CD18, CD11b and the neutrophil platelet receptor P-selectin glycoprotein ligand-1 (PSGL-1) observed in the immature LDN population (Figure 4I-K). The surface expression of the integrin CD24 (Figure S1) was not altered and CD40 was not detected across all neutrophil populations (data not shown).

The presence of neutrophil platelet aggregates in patients with COVID-19 ARDS led us to question why neutrophils were binding to activated platelets, and whether there was evidence that neutrophils themselves were becoming inappropriately activated in the blood. Neutrophils express a plethora of cell surface receptors to enable them to respond to noxious stimuli. A key element of this response is the highly regulated release of cytotoxic granule proteins. However, inappropriate degranulation in the lung tissue during ARDS is associated with epithelial and vascular damage which in turn potentiates lung injury (Grommes and Soehnlein, 2011). In health, the release of toxic granules by neutrophils in the circulation is limited by the requirement of a second activation stimulus following neutrophil priming (Vogt et al., 2018). Comparison of the proteomes of NDN populations reveals that granule cargo proteins are highly abundant and account for 20% of the neutrophil protein mass (Figure 5A). In both COVID-19 and non-COVID-19 ARDS whilst we observe an equivalent abundance of primary, secondary and tertiary granule membrane proteins (Figure S2) there is a relative reduction in the abundance of the granule cargo proteins within these circulating cells (Figure 5B). Survey of these individual proteases reveals these changes to be modest, but to occur across the different granule compartments and to be amplified in COVID-19 (Figure 5C-J). To address whether this relative reduction in intra-cellular granule protein content was consequent upon

neutrophil degranulation, we quantified surface expression of CD63, a protein known to be externalised upon degranulation. We observed a significant increase in CD63 expression which was specific to the COVID-19 neutrophils (Figure 5K), and associated with a concomitant increase in Granulocyte-macrophage colony-stimulating factor receptor alpha (GM-CSF-R-α) (Figure 5L), one of the key regulators of neutrophil degranulation. Importantly an increase in serum levels of the neutrophil granule proteins myeloperoxidase (MPO), lactoferrin and elastase in the COVID-19 ARDS patient cohort (Figure 5M-O) confirmed a phenotype of enhanced circulating neutrophil degranulation in the COVID-19 ARDS patient cohort.

Activation of neutrophil type I interferon signalling pathways and antigen presentation in COVID-19

Type I IFN are a group of cytokines which characterise the anti-viral response but are also implicated in inflammatory disease and in malignancy. Their role in COVID-19 is complex and is likely to vary depending on the stage of disease. IFNβ has been trialled as a potential treatment in the early stages in combination with other anti-viral therapies (Hung et al., 2020; Synairgen, 2020). Conversely, persistent high levels of circulating type I IFN are associated with more severe disease in the late stages of disease (Lucas et al., 2020), thought to be due to dysfunctional inflammation rather than uncontrolled viral infection. With a type I IFN signature identified by pathway analysis within the COVID-19 ARDS neutrophils and evidence that in a tumour setting, type I IFNs can regulate neutrophil functions (Pylaeva et al., 2016) we surveyed the abundance of proteins involved in anti-viral responses downstream of IFNα/β receptor (IFNAR). This revealed across the pathway a greater abundance of proteins important for type I IFN signalling and anti-viral responses in COVID-19 ARDS neutrophils including 2',5'-oligoadenylate synthetase (OAS) proteins which activate RNase L, Eukaryotic

Translation Initiation Factor 2-alpha Kinase 2 (EIF2AK) which inhibits viral transcription and the GTP binding Mx proteins which inhibit viral replication (Figure 6A-E).

Another important effect of interferon signalling in viral infection is to stimulate antigen presentation of intracellular (i.e. viral) antigens via the proteosome to alert T-cells to the infected cell. Analysis of the antigen presentation and processing pathway showed preserved levels of the immunoproteasome subunits in COVID-19 neutrophils (Figure S3), but a global increase in the expression of proteins implicated in immune cell development, regulation, antigen processing and presentation (Figure 6F) including a greater copy number of the Transporter Associated with Antigen Processing (TAP) proteins required for transport into the endoplasmic reticulum for loading onto class I Major Histocompatibility Complex (MHC) molecules (Figure 6G-H), and in class I MHC molecules (Figure 6I-K).

Metabolic rewiring of COVID-19 ARDS neutrophils and changes in neutrophil metabolism in response to type I interferon

Type I IFNs have been found to drive metabolic adaptations in plasmacytoid dendritic cells (pDC) with upregulation of fatty acid oxidation and oxidative phosphorylation promoting pDC activation in response to Toll-Like Receptor (TLR) 9 agonists (Wu et al., 2016). In light of the observed type I IFN COVID-19 signature, we questioned whether in disease circulating neutrophils re-wire their core metabolic processes to maintain energy requirements, and if these metabolic adaptations were IFN mediated. In keeping with the previously reported reliance of neutrophils on glycolysis for ATP production, disease neutrophils retained expression of glucose transporters (GLUT1 and GLUT3, Figure S4A) and glycolytic enzymes (Figure S4B-C). However, COVID-19 ARDS neutrophils demonstrated an increase in intracellular levels of free glucose (Figure 7A), despite normal plasma glucose levels (Figure 7B) and preserved

levels of intracellular glycogen (Figure 7C), raising the possibility that neutrophils in COVID-19 ARDS have reduced glycolytic flux. This was associated with increased abundance of the Tricarboxylic Acid (TCA) cycle intermediaries Acetyl Coenzyme A (acetyl CoA), citrate and malate (Figure 7D). Despite this, COVID-19 ARDS neutrophils showed preserved energy status (Figure 7E) with access to free glutamine, preservation of glutaminase and increased intracellular glutamate that together support the proposed shift from glycolysis and rewiring of their metabolic programme (Figure 7F, S4C-D). To address whether direct stimulation of neutrophils with type I IFN was sufficient to reprogram neutrophil metabolism, blood neutrophils from healthy controls were activated in the presence or absence of IFNα and IFN1β and glycolysis was assessed by extracellular flux analysis (Figure S4E). In keeping with diminished flux through glycolysis in COVID-19 ARDS neutrophils, exposure to IFN caused a significant reduction in the glycolytic reserve of N-Formylmethionine-leucyl-phenylalanine (fMLP)-stimulated neutrophils (Figure 7G, S4F).

To directly address whether neutrophil recognition of viral ssRNA via TLR family members 7 and 8, was important for mediating the type I IFN pro-inflammatory neutrophil responses we observe in COVID-19, healthy control neutrophils were stimulated with the TLR7/8 agonist resiquimod. In hypoxic culture conditions, resiquimod activated neutrophils with shedding of CD62L (Figure 7H), and upregulation of CD66b and CD63 (Figure 7I-J). Resiquimod also up-regulated neutrophil expression of both components of the Mac-1 platelet binding complex, CD11b and CD18 (Figure7 K-L) replicating the observed phenotype of COVID-19.

Discussion

In this study the direct comparison of peripheral blood neutrophil populations from patients with COVID-19 and non-COVID-19 ARDS allows us to identify processes that are specific to

and exaggerated in patients with ARDS in the context of infection with SARS-CoV-2. Whilst the expansion of neutrophil populations and the presence of LDN subsets previously reported in COVID-19 are also observed in non-COVID-19 ARDS, platelet degranulation and activation of type I IFN responses are specific to COVID-19 ARDS.

A striking clinical divergence between COVID-19 and non-COVID-19 ARDS is the prominence of micro and macrovascular thrombosis in COVID-19 ARDS. The presence of neutrophil-platelet aggregates, in addition to the proteomic signatures indicative of platelet degranulation and clotting cascade activation implicate neutrophils in the pathogenesis of immune clot formation. Whether neutrophil activation facilitates the formation of neutrophil platelet aggregates, impairing neutrophil transmigration and directly contributing to vascular damage and to the formation of microthrombi through the release of neutrophil extracellular traps (NETs) as recently suggested (Radermecker et al., 2020; Veras et al., 2020) or by alternative mechanisms requires further exploration. It is certainly interesting to note that at post-mortem, and in marked contrast to non-COVID-19 ARDS, patients with COVID-19 have a paucity of neutrophils in the alveoli despite diffuse alveolar damage. It will also be important to dissect whether the uplift in expression of proteins associated with fibrin clot formation in COVID-19 ARDS is consequent upon intrinsic neutrophil expression of these proteins, neutrophil processing of platelet proteins or reflective of adherent platelets contributing to the protein signatures of the circulating neutrophil populations.

The importance of neutrophil activation of type I IFN signalling pathways in COVID-19 ARDS also requires further consideration given the disconnect between tissue injury and viral detection (Dorward et al., 2020). The ability of neutrophils to cross-present exogenous antigens to CD8+ T cells has previously been reported and is highly relevant for T cell priming

in vivo (Pufnock et al., 2011). This may be particularly relevant in a disease where early CD4+ and CD8+ T cell responses against SARS-CoV-2 are thought to be protective (Blanco-Melo et al., 2020; Grifoni et al., 2020), but late responses associated with damaging inflammation (Chen et al., 2020; Grifoni et al., 2020; Li et al., 2008; Liu et al., 2019). Whilst activation of anti-viral responses including class I MHC antigen presentation would therefore appear beneficial with respect to viral control, if this is associated with a hyper-inflammatory neutrophil phenotype and delayed T cell activation, the net consequence could be one of ongoing tissue injury. In this regard, we would predict that inappropriate degranulation of neutrophils in the circulation would be highly damaging and cause wide-spread vascular inflammation within the microvasculature where neutrophils are known to be sequestered. Our evidence of expanded neutrophil numbers together with increased neutrophil activation and degranulation and detection of serum neutrophil granule proteins in patients with COVID-19 ARDS would support this concept of a hyper-inflammatory damaging circulating innate response. It will be interesting to assess whether the early benefit of IFN treatment in COVID-19 (Synairgen, 2020) is lost in late disease as a consequence of this aberrant IFN mediated innate immune response.

The mechanism by which type I IFN regulates neutrophil behaviour remains to be fully elucidated. In plasmacytoid dendritic cells, TLR 9 mediated activation is dependent upon autocrine production of type I IFNs and an increase in oxidative metabolism (Wu et al., 2016). Neutrophils are unique in their reliance on non-oxidative metabolism for ATP production, even when oxygen is freely available. It is therefore of interest that in response to IFNα and IFNβ, neutrophils rewire their metabolic programme by reducing their glycolytic potential in keeping with the phenotype observed in NDN from patients with COVID-19 ARDS. Together with an increase in detectable levels of glutamate and TCA cycle intermediaries, especially malate, this

raises the interesting possibility that neutrophils undergo alternative substrate utilisation via oxidative metabolism. Future work will be required to understand whether such alternative substrate utilisation occurs and how this potentiates anti-viral and pro-inflammatory innate immune responses following viral challenge.

In summary, we provide evidence of a dysregulated circulating neutrophil response in COVID-19, with activation of components of the neutrophil type I IFN responses in patients who develop ARDS. This hyperinflammatory state is associated with metabolic rewiring of the neutrophils, neutrophil degranulation and the formation of neutrophil platelet aggregates in the blood. Strategies to target damaging innate immune responses following infection with SARS-CoV-2 will likely be required in developing an effective therapeutic arsenal for COVID-19 ARDS.

Acknowledgements

This research was supported by a Wellcome Trust Senior Clinical Fellowship award (209220) and a CRUK cancer immunology project award (C62207/A24495) to S.R.W, Wellcome Clinical training Fellowship awards to T.M. (214383/Z/18/Z) and E.R.W (108717/Z/15/Z), a Wellcome Trust Post-doctoral Training Clinical Fellowship awarded to A.S.M (110086), a Medical Research Foundation PhD Studentship to S.A., UKRI/NIHR funding through the UK Coronavirus Immunology Consortium (UK-CIC) and a CSO grant (COV/DUN/20/01) to D.A.C, and a LifeArc STOPCOVID award to A.P and S.M. We thank the CIR blood resource (AMREC no. 15-HV-013) for the recruitment of blood from healthy donors and the clinical support teams, patients and their families that have contributed to this study. Many thanks to the QMRI Flow Cytometry & Cell Sorting Facility, Edinburgh University (Will Ramsay and

Mari Pattison) and CALM Facility, Edinburgh University (Rolly Wiegand and Kseniya Korobchevskaya) for their expertise and assistance.

Author Contributions

L.R, M.A.S.G, T.M, A.J.M.H, E.W, S.A, P.S, P.C, A.S.M, D.H, S.K.C, J.S, S.J, R.G, A.P, S.M, I.H, M.H.F, A.B, S.P, A.L, G.R.B, B.G, W.V, C.T.C performed the research. L.R, M.A.S.G, T.M, A.J.M.H, M.K.W, D.G, D.A.C, S.R.W interpreted the data. L.R, M.A.S.G, T.M, A.J.M.H, M.H.F, K.D, N.H, D.D, M.K.W, D.G, D.A.C, S.R.W designed the research. L.R, M.A.S.G, T.M, A.J.M.H, E.W, A.K., M.K.W, D.G, D.A.C, S.R.W provided expertise and feedback. L.R, M.A.S.G, T.M, A.J.M.H, E.W, D.A.C, S.R.W wrote the manuscript.

Declaration of Interests

The authors declare no competing interests.

STAR ★ Methods

RESOURCE AVAILABILITY

Lead Contact

Further information and requests for resources and reagents should be directed to and will be fulfilled by the Lead Contact, Sarah Walmsley (sarah.walmsley@ed.ac.uk).

Materials Availability

This study did not generate new unique reagents.

Data and Code Availability

Raw mass spectrometry data files and Spectronaut analysis files will be available to download from the ProteomeXchange data repository (http://proteomecentral.proteomexchange.org/cgi/GetDataset) at the time of publication.

EXPERIMENTAL MODEL AND SUBJECT DETAILS

Healthy donor and patient recruitment

Human peripheral venous blood was taken from healthy volunteers with written informed consent obtained from all participants prior to sample collection as approved by the University of Edinburgh Centre for Inflammation Research Blood Resource Management Committee (AMREC 15-HV-013). The collection of peripheral venous blood from male or female patients diagnosed with COVID-19 and/or presenting with ARDS was approved by Scotland A Research Ethics Committee. Patient recruitment took place from April 2020 through August 2020 from The Royal Infirmary of Edinburgh, Scotland, UK through the ARDS Neut (20/SS/0002) and CASCADE (20/SS/0052) Study, with informed consent obtained by proxy.

Cell Culture

NDN obtained from the PMN layer of healthy donors were resuspended at 5×10^6/mL in Roswell Park Memorial Institute (RPMI) 1640 (Gibco) with 10% dialyzed foetal calf serum (Gibco) and 50 U/mL streptomycin and penicillin in normoxia (19 kPa) or hypoxia (3 kPa) at 5% CO_2 as previously described (Walmsley et al., 2011). Cells were cultured in the absence or presence of IFNα/ IFNβ (500 units/mL) and/or resiquimod (15 μM, Sigma-Aldrich) for the indicated time prior to harvest.

METHOD DETAILS

Isolation of human peripheral blood neutrophils

Up to 80 mL of whole blood was collected into citrate tubes. An aliquot of 5 mL of whole blood was treated with red cell lysis buffer (Invitrogen) and with the remaining volume, human blood leukocytes were isolated by dextran sedimentation and discontinuous Percoll gradients as described by (Haslett et al., 1985).

Flow cytometry

Lysed whole blood, PMN and PBMC layers isolated from Percoll gradients, as well as NDN treated with or without IFN/resiquimod for 1 h were stained with Zombie Aqua™ Fixable viability dye (1:400) (Biolegend) to exclude dead cells from analysis. Cells were subsequently treated with Human TruStain FcX™ (1:100) (Biolegend) and stained for 30 min on ice with antibodies listed in the Key Resources Table with appropriate fluorescence minus one (FMO) controls. Cells were then washed and fixed with 4% paraformaldehyde (PFA) and acquired using BD LSRFortessa™ flow cytometer (Beckton Dickinson). Compensation was performed using BD FACSDiva™ software version 8.0 and data analysed in FlowJo version 10.2. Gating strategy to identify neutrophils, maturity and surface expression of various markers are outlined in Figure S5. Samples with neutrophil purity of <95% (CD66b+CD49d-) were excluded from analysis.

Fluorescence activated cell sorting (FACS) of NDN and LDN

PMN and PBMC layers isolated from Percoll gradients were fixed with 1.5% PFA. FACS of NDN and LDN from PMN and PBMC layers respectively were performed using BD FACSAria™ Fusion flow cytometer fitted with a 70 µm nozzle and running BD FACSDiva™ software version 8.0 (Beckton Dickinson). Singlets were gated according to forward scatter height vs. forward scatter area (FSC-H vs. FSC-A) and side scatter height vs. side scatter area (SSC-H vs. SSC-A) parameters and NDN and LDN identified according to forward vs. side

scatter (FSC vs. SSC) parameters. NDN and LDN were collected at 4 °C in 15 mL Falcon tubes pre-coated with Dulbecco's phosphate-buffered saline (DPBS; Thermo Fisher).

Cell immunostaining for microscopy

NDN and LDN were isolated by FACS as described. Cells were pelleted and blocked with Fc Receptor Blocking Solution followed by staining with anti-CD41 antibody (Biolegend) and counterstaining with propidium iodide (Biolegend) according to manufacturer's guidelines. Multichamber slides (Ibidi) were used to image the samples in a confocal microscope (Leica SP8). Image acquisition was performed at 63x magnification with the same settings across all images. Fiji software was used to process the images (Schindelin et al., 2012). Scale bars depict 5 μm.

Measurement of granule protein levels

Enzyme-linked immunosorbent assay (ELISA) was performed according to manufacturer's protocol to quantify MPO, lactoferrin and elastase levels (Abcam) in plasma from healthy donors and non-COVID-19 ARDS and COVID-19 patients.

Measurement of intracellular glycogen stores

1×10^6 NDN were lysed in 200 μL ultrapure H_2O, boiled for 5 min at 100 °C and stored at –80 °C. Lysates were then centrifuged at 18,000 × g for 10 min at 4°C to remove cell debris and glycogen content was measure using a fluorometric assay (Sigma-Aldrich).

Proteomics sample preparation

For non-fixed cells proteomics, 2×10^6 neutrophils isolated from PMN and PBMC layers by FACS were centrifuged at 340 × g for 5 min at 4 °C, with pellets resuspended in 400 μL of freshly made 5% sodium dodecyl sulfate (SDS) lysis buffer and vortexed. Samples were then

heat denatured in a heat block for 5 min at 100 °C and stored at –80 °C. Cell pellets were lysed in 5% SDS, 10 mM tris(2-carboxyethyl) phosphine hydrochloride and 50 mM tetraethylammonium bromide. Lysates were shaken at 500 rpm at 22 °C for 5 min before being incubated at 98 °C for 5 min. Samples were allowed to cool and were then sonicated with a BioRuptor (30 cycles: 30 s on and 30 s off). Tubes were centrifuged at 17,000 × g to collect the cell lysate and 1 μL of benzonase (27.8 units) was added to each sample and samples incubated at 37 °C for 15 min. Samples were then alkylated with addition of 20 mM iodoacetamide for 1 h at 22 °C in the dark. Protein lysates were processed for mass spectrometry using s-trap spin columns following the manufacturer's instructions (Protifi) (HaileMariam et al., 2018). Lysates were digested with Trypsin at a ratio 1:20 (protein:enzyme) in 50 mM ammonium bicarbonate. Peptides were eluted from s-trap columns by sequentially adding 80 μL of 50 mM ammonium bicarbonate followed by 80 μL of 0.2 % formic acid with a final elution using 80 μL of 50 % acetonitrile + 0.2 % formic acid.

Fixed cell samples were processed using the in-cell digest method (Kelly et al., 2020). Cells were pelleted by centrifugation and washed in PBS to remove methanol. Cells were resuspended in 400 μL digest buffer (0.1 M TEAB + 1 mM MgCl2 + 5 μL benzonase (27.8 units/μL), pH 8) and incubated at 37 °C for 20 min. 12.5 μg trypsin was added to each sample and samples incubated at 37 °C for 18 h. After this incubation, an additional 12.5 μg of trypsin was added to each sample and samples incubated at 37 °C for 1 h. Digested peptides were desalted using Pierce peptide desalting columns. Peptides from s-trap and in-cell digest method were dried in vacuo and suspended in 5% formic acid for LC-MS analysis.

LC-MS analysis

For each sample, 2 µg of peptide was analysed on a Q-Exactive-HF-X (Thermo Scientific) mass spectrometer coupled with a Dionex Ultimate 3000 RS (Thermo Scientific). LC buffers were the following: buffer A (0.1% formic acid in Milli-Q water (v/v)) and buffer B (80% acetonitrile and 0.1% formic acid in Milli-Q water (v/v)). 2 µg aliquot of each sample were loaded at 15 µL/min onto a trap column (100 µm × 2 cm, PepMap nanoViper C18 column, 5 µm, 100 Å, Thermo Scientific) equilibrated in 0.1% trifluoroacetic acid (TFA). The trap column was washed for 3 min at the same flow rate with 0.1% TFA then switched in-line with a Thermo Scientific, resolving C18 column (75 µm × 50 cm, PepMap RSLC C18 column, 2 µm, 100 Å). The peptides were eluted from the column at a constant flow rate of 300 nl/min with a linear gradient from 3% buffer B to 6% buffer B in 5 min, then from 6% buffer B to 35% buffer B in 115 min, and finally to 80% buffer B within 7 min. The column was then washed with 80% buffer B for 4 min and re-equilibrated in 3% buffer B for 15 min. Two blanks were run between each sample to reduce carry-over. The column was kept at a constant temperature of 50 ^{o}C at all times.

The data was acquired using an easy spray source operated in positive mode with spray voltage at 1.9 kV, the capillary temperature at 250 ^{o}C and the funnel RF at 60 ^{o}C. The MS was operated in DIA mode as reported earlier (Muntel et al., 2019) with some modifications. A scan cycle comprised a full MS scan (m/z range from 350-1650, with a maximum ion injection time of 20 ms, a resolution of 120 000 and automatic gain control (AGC) value of 5×10^6). MS survey scan was followed by MS/MS DIA scan events using the following parameters: default charge state of 3, resolution 30.000, maximum ion injection time 55 ms, AGC $3x10^6$, stepped normalized collision energy 25.5, 27 and 30, fixed first mass 200 m/z. The inclusion list (DIA windows) and windows widths are shown in Table S2. Data for both MS and MS/MS scans were acquired in profile mode. Mass accuracy was checked before the start of samples analysis.

Analysis of proteomics data

The DIA data were analyzed with Spectronaut 14 using the directDIA option (Bruderer et al., 2015). Cleavage Rules were set to Trypsin/P, Peptide maximum length was set to 52 amino acids, Peptide minimum length was set to 7 amino acids and Missed Cleavages set to 2. Calibration Mode was set to Automatic. Search criteria included carbamidomethylation of cysteine as a fixed modification, as well as oxidation of methionine, deamidation of asparagine and glutamine and acetylation (protein N-terminus) as variable modifications. The FDR threshold was set to 1% Q-value at both the Precursor and Protein level. The single hit definition was to Stripped sequence. The directDIA data were searched against the human SwissProt database (July 2020) and included isoforms. The Major Group Quantity was set to the Sum of peptide quantity and the Minor Group Quantity was set to the Sum of the precursor quantity, Cross Run Normalization was disabled. Fold changes and P-values were calculated in R utilising the bioconductor package LIMMA version 3.7 (Ritchie et al., 2015). The Q-values provided were generated in R using the "qvalue" package version 2.10.0. Estimates of protein copy numbers per cell were calculated using the histone ruler method (Wisniewski et al., 2014). The mass of individual proteins was estimated using the following formula: CN × MW/NA = protein mass (g $cell^{-1}$), where CN is the protein copy number, MW is the protein molecular weight (in Da) and NA is Avogadro's Constant.

Metabolomic analysis

2.5×10^6 neutrophils isolated from the PMN layer were centrifuged at 340 × g for 5 min at 4 °C, with pellets resuspended in 100 µL of 80% methanol. Following extraction, samples were stored at –80 °C. Relative metabolite abundance was determined using ion-pairing RP-HPLC coupled to a Q-Exactive Orbitrap Mass Spectrometer and data acquired using Xcalibur

Software in negative mode. Data were analysed in a targeted manner, using Xcalibur against an in-house compound library to obtain the area under the curve at the expected retention time and the average of two replicate samples subjected to further analysis. PCA analysis was performed in R by prcomp and visualised with the "ggbiplot" package version 0.55. Individual metabolites were expressed relative to the mean of the healthy control population and analysed in Prism 8.00 (Graphpad Software Inc). Adenylate charge was determined as previously described (Sadiku et al., 2017).

Extracellular flux analysis

Neutrophils cultured in normoxia for 4 h in the presence or absence of IFNα/ IFNβ were harvested and washed in warm saline. Cells were resuspended at 3×10^6/mL in XF DMEM pH 7.4 (Agilent), supplemented with 2 mM glutamine and IFNα/IFNβ added to the appropriate cells at the concentrations described previously. 3×10^6 neutrophils were seeded into each well of a 24-well cell culture microplate (Agilent) to give at least duplicate samples per condition and 4 wells were left as media controls. After 45 min in a CO_2-free incubator, the plate was loaded into a Seahorse XFe 24 Analyzer (Agilent). Cells were sequentially treated by injection of glucose (10 mM, Sigma), oligomycin A (1 μM, Sigma) and 2-deoxyglucose (50 mM, Sigma). Oxygen consumption rate (OCR) and extracellular acidification rates (ECAR) were analysed in Agilent Seahorse Analytics for each plate before exporting to GraphPad to pool for final analysis.

QUANTIFICATION AND STATISTICAL ANALYSIS

Statistical tests were performed using Prism 8.00 software (GraphPad Software Inc). Data was tested for normality using Shapiro-Wilk test, with significance testing detailed in figure legends. Significance was defined as a p value of <0.05 after correction for multiple

comparisons where applicable. Sample sizes are shown in figure legends, with each n number representing a different blood donor for human cells.

Key Resources Table

Antibody	Clone	Catalogue number	Fluorophore	Source	Concentration
CD16	eBioCB16	11-0168-42	FITC	Ebioscience	1:100
CD63	H5C6	353004	PE	Biolegend	1:100
CD10	K036C2	357212	PE-Cy7	Biolegend	1:100
CD66b	G10F5	305114	AF700	Biolegend	1:100
CD62L	DREG-56	304814	APC-Cy7	Biolegend	1:100
CD11b	M1/70	101243	BV785	Biolegend	1:400
CD49d	9F10	310714	BV421	Biolegend	1:100
GM-CSF-R-α	hGMCSFR -M1	747410	BV750	BD Biosciences	1:400
CD18	TS1/18	302117	PE-Cy7	Biolegend	1:100
PSGL-1	KPL-1	328811	APC	Biolegend	1:100
CD40	5C3	334323	APC-Cy7	Biolegend	1:100
CD41	HIP8	303729	BV421	Biolegend	1:100
CD24	ML5	311123	BV605	Biolegend	1:100

References

1. ARDS Network., Brower, R.G., Matthay, M.A., Morris, A., Schoenfeld, D., Thompson, B.T., and Wheeler, A. (2000). Ventilation with lower tidal volumes as compared with traditional tidal volumes for acute lung injury and the acute respiratory distress syndrome. The New England journal of medicine *342*, 1301-1308.
2. ARDS Task Force, Ranieri, V.M., Rubenfeld, G.D., Thompson, B.T., Ferguson, N.D., Caldwell, E., Fan, E., Camporota, L., and Slutsky, A.S. (2012). Acute respiratory distress syndrome: the Berlin Definition. JAMA *307*, 2526-2533.
3. Bachofen, M., and Weibel, E.R. (1977). Alterations of the gas exchange apparatus in adult respiratory insufficiency associated with septicemia. Am Rev Respir Dis *116*, 589-615.
4. Blanco-Melo, D., Nilsson-Payant, B.E., Liu, W.C., Uhl, S., Hoagland, D., Moller, R., Jordan, T.X., Oishi, K., Panis, M., Sachs, D.*, et al.* (2020). Imbalanced Host Response to SARS-CoV-2 Drives Development of COVID-19. Cell *181*, 1036-1045 e1039.
5. Bruderer, R., Bernhardt, O.M., Gandhi, T., Miladinovic, S.M., Cheng, L.Y., Messner, S., Ehrenberger, T., Zanotelli, V., Butscheid, Y., Escher, C.*, et al.* (2015). Extending the limits of quantitative proteome profiling with data-independent acquisition and application to acetaminophen-treated three-dimensional liver microtissues. Mol Cell Proteomics *14*, 1400-1410.
6. Chen, G., Wu, D., Guo, W., Cao, Y., Huang, D., Wang, H., Wang, T., Zhang, X., Chen, H., Yu, H.*, et al.* (2020). Clinical and immunological features of severe and moderate coronavirus disease 2019. The Journal of clinical investigation *130*, 2620-2629.
7. Dorward, D.A., Russell, C.D., Um, I.H., Elshani, M., Armstrong, S.D., Penrice-Randal, R., Millar, T., Lerpiniere, C.E., Tagliavini, G., Hartley, C.S.*, et al.* (2020). Tissue-specific tolerance in fatal Covid-19. medRxiv.

8. Dreyfuss, D., and Saumon, G. (1993). Role of tidal volume, FRC, and end-inspiratory volume in the development of pulmonary edema following mechanical ventilation. Am Rev Respir Dis *148*, 1194-1203.
9. Eltzschig, H.K., and Carmeliet, P. (2011). Hypoxia and inflammation. The New England journal of medicine *364*, 656-665.
10. Flick, M.R., Perel, A., and Staub, N.C. (1981). Leukocytes are required for increased lung microvascular permeability after microembolization in sheep. Circulation research *48*, 344-351.
11. Grifoni, A., Weiskopf, D., Ramirez, S.I., Mateus, J., Dan, J.M., Moderbacher, C.R., Rawlings, S.A., Sutherland, A., Premkumar, L., Jadi, R.S.*, et al.* (2020). Targets of T Cell Responses to SARS-CoV-2 Coronavirus in Humans with COVID-19 Disease and Unexposed Individuals. Cell *181*, 1489-1501 e1415.
12. Groll, D.L., To, T., Bombardier, C., and Wright, J.G. (2005). The development of a comorbidity index with physical function as the outcome. J Clin Epidemiol *58*, 595-602.
13. Grommes, J., and Soehnlein, O. (2011). Contribution of neutrophils to acute lung injury. Mol Med *17*, 293-307.
14. HaileMariam, M., Eguez, R.V., Singh, H., Bekele, S., Ameni, G., Pieper, R., and Yu, Y. (2018). S-Trap, an Ultrafast Sample-Preparation Approach for Shotgun Proteomics. J Proteome Res *17*, 2917-2924.
15. Haslett, C., Guthrie, L.A., Kopaniak, M.M., Johnston, R.B., Jr., and Henson, P.M. (1985). Modulation of multiple neutrophil functions by preparative methods or trace concentrations of bacterial lipopolysaccharide. The American journal of pathology *119*, 101-110.

16. Howden, A.J.M., Hukelmann, J.L., Brenes, A., Spinelli, L., Sinclair, L.V., Lamond, A.I., and Cantrell, D.A. (2019). Quantitative analysis of T cell proteomes and environmental sensors during T cell differentiation. Nat Immunol *20*, 1542-1554.
17. Huang, C., Wang, Y., Li, X., Ren, L., Zhao, J., Hu, Y., Zhang, L., Fan, G., Xu, J., Gu, X.*, et al.* (2020). Clinical features of patients infected with 2019 novel coronavirus in Wuhan, China. Lancet *395*, 497-506.
18. Hung, I.F., Lung, K.C., Tso, E.Y., Liu, R., Chung, T.W., Chu, M.Y., Ng, Y.Y., Lo, J., Chan, J., Tam, A.R.*, et al.* (2020). Triple combination of interferon beta-1b, lopinavir-ritonavir, and ribavirin in the treatment of patients admitted to hospital with COVID-19: an open-label, randomised, phase 2 trial. Lancet *395*, 1695-1704.
19. Kelly, V., al-Rawi, A., Lewis, D., and Ly, T. (2020). Cell cycle state proteomics and classification using in-cell protease digests and mass spectrometry. medRxiv.
20. Knaus, W.A., Draper, E.A., Wagner, D.P., and Zimmerman, J.E. (1985). APACHE II: a severity of disease classification system. Critical care medicine *13*, 818-829.
21. Li, C.K., Wu, H., Yan, H., Ma, S., Wang, L., Zhang, M., Tang, X., Temperton, N.J., Weiss, R.A., Brenchley, J.M.*, et al.* (2008). T cell responses to whole SARS coronavirus in humans. Journal of immunology *181*, 5490-5500.
22. Liu, J., Liu, Y., Xiang, P., Pu, L., Xiong, H., Li, C., Zhang, M., Tan, J., Xu, Y., Song, R.*, et al.* (2020). Neutrophil-to-lymphocyte ratio predicts critical illness patients with 2019 coronavirus disease in the early stage. J Transl Med *18*, 206.
23. Liu, L., Wei, Q., Lin, Q., Fang, J., Wang, H., Kwok, H., Tang, H., Nishiura, K., Peng, J., Tan, Z.*, et al.* (2019). Anti-spike IgG causes severe acute lung injury by skewing macrophage responses during acute SARS-CoV infection. JCI Insight *4*.

24. Lucas, C., Wong, P., Klein, J., Castro, T.B.R., Silva, J., Sundaram, M., Ellingson, M.K., Mao, T., Oh, J.E., Israelow, B.*, et al.* (2020). Longitudinal analyses reveal immunological misfiring in severe COVID-19. Nature *584*, 463-469.

25. Muntel, J., Gandhi, T., Verbeke, L., Bernhardt, O.M., Treiber, T., Bruderer, R., and Reiter, L. (2019). Surpassing 10 000 identified and quantified proteins in a single run by optimizing current LC-MS instrumentation and data analysis strategy. Mol Omics *15*, 348-360.

26. Pufnock, J.S., Cigal, M., Rolczynski, L.S., Andersen-Nissen, E., Wolfl, M., McElrath, M.J., and Greenberg, P.D. (2011). Priming CD8+ T cells with dendritic cells matured using TLR4 and TLR7/8 ligands together enhances generation of CD8+ T cells retaining CD28. Blood *117*, 6542-6551.

27. Pylaeva, E., Lang, S., and Jablonska, J. (2016). The Essential Role of Type I Interferons in Differentiation and Activation of Tumor-Associated Neutrophils. Front Immunol *7*, 629.

28. Riffelmacher, T., Clarke, A., Richter, F.C., Stranks, A., Pandey, S., Danielli, S., Hublitz, P., Yu, Z., Johnson, E., Schwerd, T.*, et al.* (2017). Autophagy-Dependent Generation of Free Fatty Acids Is Critical for Normal Neutrophil Differentiation. Immunity *47*, 466-480 e465.

29. Ritchie, M.E., Phipson, B., Wu, D., Hu, Y., Law, C.W., Shi, W., and Smyth, G.K. (2015). limma powers differential expression analyses for RNA-sequencing and microarray studies. Nucleic Acids Res *43*, e47.

30. Sadiku, P., Willson, J.A., Dickinson, R.S., Murphy, F., Harris, A.J., Lewis, A., Sammut, D., Mirchandani, A.S., Ryan, E., Watts, E.R.*, et al.* (2017). Prolyl hydroxylase 2 inactivation enhances glycogen storage and promotes excessive neutrophilic responses. J Clin Invest *127*, 3407-3420.

31. Schindelin, J., Arganda-Carreras, I., Frise, E., Kaynig, V., Longair, M., Pietzsch, T., Preibisch, S., Rueden, C., Saalfeld, S., Schmid, B., *et al.* (2012). Fiji: an open-source platform for biological-image analysis. Nat Methods *9*, 676-682.
32. Schulte-Schrepping, J., Reusch, N., Paclik, D., Bassler, K., Schlickeiser, S., Zhang, B., Kramer, B., Krammer, T., Brumhard, S., Bonaguro, L., *et al.* (2020). Severe COVID-19 Is Marked by a Dysregulated Myeloid Cell Compartment. Cell.
33. Silvestre-Roig, C., Fridlender, Z.G., Glogauer, M., and Scapini, P. (2019). Neutrophil Diversity in Health and Disease. Trends Immunol *40*, 565-583.
34. Synairgen (2020). Synairgen announces positive results from trial of SNG001 in hospitalised COVID-19 patients. (Southampton, Synairgen plc).
35. Tian, S., Xiong, Y., Liu, H., Niu, L., Guo, J., Liao, M., and Xiao, S.Y. (2020). Pathological study of the 2019 novel coronavirus disease (COVID-19) through postmortem core biopsies. Mod Pathol *33*, 1007-1014.
36. Tobin, M.J. (2020). Basing Respiratory Management of COVID-19 on Physiological Principles. Am J Respir Crit Care Med *201*, 1319-1320.
37. Vogt, K.L., Summers, C., Chilvers, E.R., and Condliffe, A.M. (2018). Priming and de-priming of neutrophil responses in vitro and in vivo. European journal of clinical investigation *48 Suppl 2*, e12967.
38. Walmsley, S.R., Chilvers, E.R., Thompson, A.A., Vaughan, K., Marriott, H.M., Parker, L.C., Shaw, G., Parmar, S., Schneider, M., Sabroe, I., *et al.* (2011). Prolyl hydroxylase 3 (PHD3) is essential for hypoxic regulation of neutrophilic inflammation in humans and mice. J Clin Invest *121*, 1053-1063.
39. Walmsley, S.R., Print, C., Farahi, N., Peyssonnaux, C., Johnson, R.S., Cramer, T., Sobolewski, A., Condliffe, A.M., Cowburn, A.S., Johnson, N., and Chilvers, E.R.

(2005). Hypoxia-induced neutrophil survival is mediated by HIF-1alpha-dependent NF-kappaB activity. The Journal of experimental medicine *201*, 105-115.

40. WHO (2020). Clinical management of COVID-19: interim guidance. (WHO Global).
41. Wisniewski, J.R., Hein, M.Y., Cox, J., and Mann, M. (2014). A "proteomic ruler" for protein copy number and concentration estimation without spike-in standards. Mol Cell Proteomics *13*, 3497-3506.
42. Wu, D., Sanin, D.E., Everts, B., Chen, Q., Qiu, J., Buck, M.D., Patterson, A., Smith, A.M., Chang, C.H., Liu, Z.*, et al.* (2016). Type 1 Interferons Induce Changes in Core Metabolism that Are Critical for Immune Function. Immunity *44*, 1325-1336.
43. Zhao, Q., Meng, M., Kumar, R., Wu, Y., Huang, J., Deng, Y., Weng, Z., and Yang, L. (2020). Lymphopenia is associated with severe coronavirus disease 2019 (COVID-19) infections: A systemic review and meta-analysis. Int J Infect Dis *96*, 131-135.

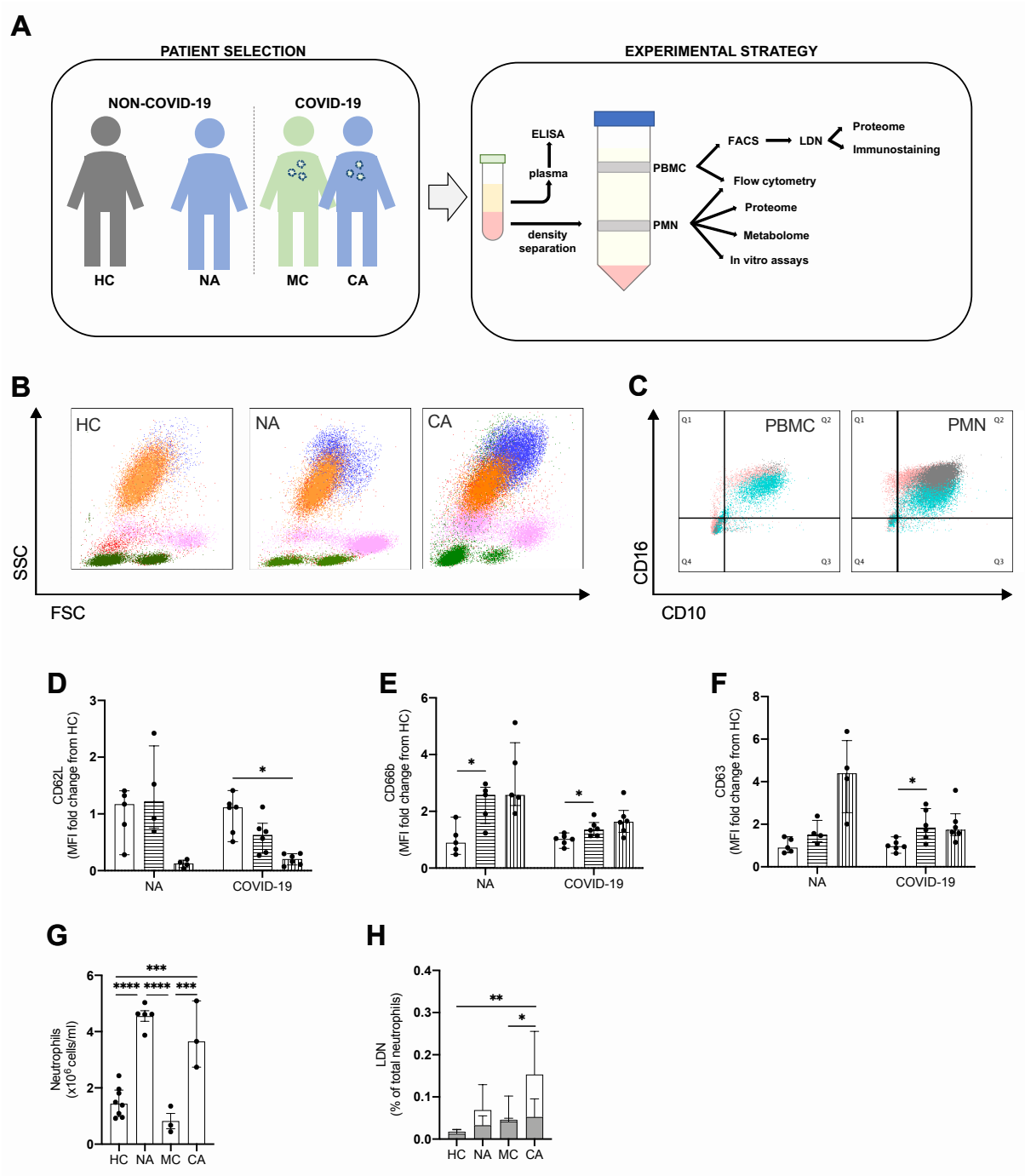

Figure 1. Circulating neutrophil populations are expanded in COVID-19 and non-COVID-19 ARDS. (A) Patient selection criteria (healthy control, HA, non-COVID-19 ARDS, NA, moderate COVID-19, MC, and COVID-19 ARDS, CA), neutrophil isolation, and workflow depicted. (B) Representative SSC vs. FSC plots of stained whole blood from HA, NA and CA displaying lymphocyte (green), monocyte (pink), mature (CD16+, orange) and

immature (CD16-, blue) neutrophil populations. (C) Representative CD16 vs. CD10 dot plots of stained polymorphonuclear (PMN) and peripheral blood mononuclear cell (PBMC) layers isolated by Percoll gradients from HC (grey), NA (blue) or CA (pink) patients. (D-F) Surface expression of neutrophil activation markers expressed as a fold change of geometric mean fluorescence intensity (MFI) from normal density neutrophils (NDN) respective to the disease state as determined by flow cytometry analysis of mature NDN (CD66b+CD16+, open bars), mature low density neutrophils (LDN) (CD66b+CD16+, horizontal striped bars) and immature LDN (CD66b+CD16-, vertical striped bars) from NA (n = 4-5) or COVID-19 (n = 6) patients. Data are mean ± SD. *$p < 0.05$, determined by repeated two-way ANOVA and Sidak's post hoc-testing. (G) Total neutrophil counts of HC (n = 7), NA (n = 3), MC (n=3) and CA (n = 3) performed by haemocytometer and differential cell count established by flow cytometry. Data are mean ± SD. ***$p < 0.001$, ****$p < 0.0001$, determined by one-way ANOVA and Holm-Sidak's post hoc-testing. (H) Proportion of mature (CD66b+CD16+CD10+, grey bars) and immature LDN (CD66b+CD16-CD10-, white bars) isolated from patient cohorts as described in (G) were measured by flow cytometry. Data are mean ± SD. *$p < 0.05$, **$p < 0.01$, determined by repeated measures two-way ANOVA and Tukey's post hoc-testing.

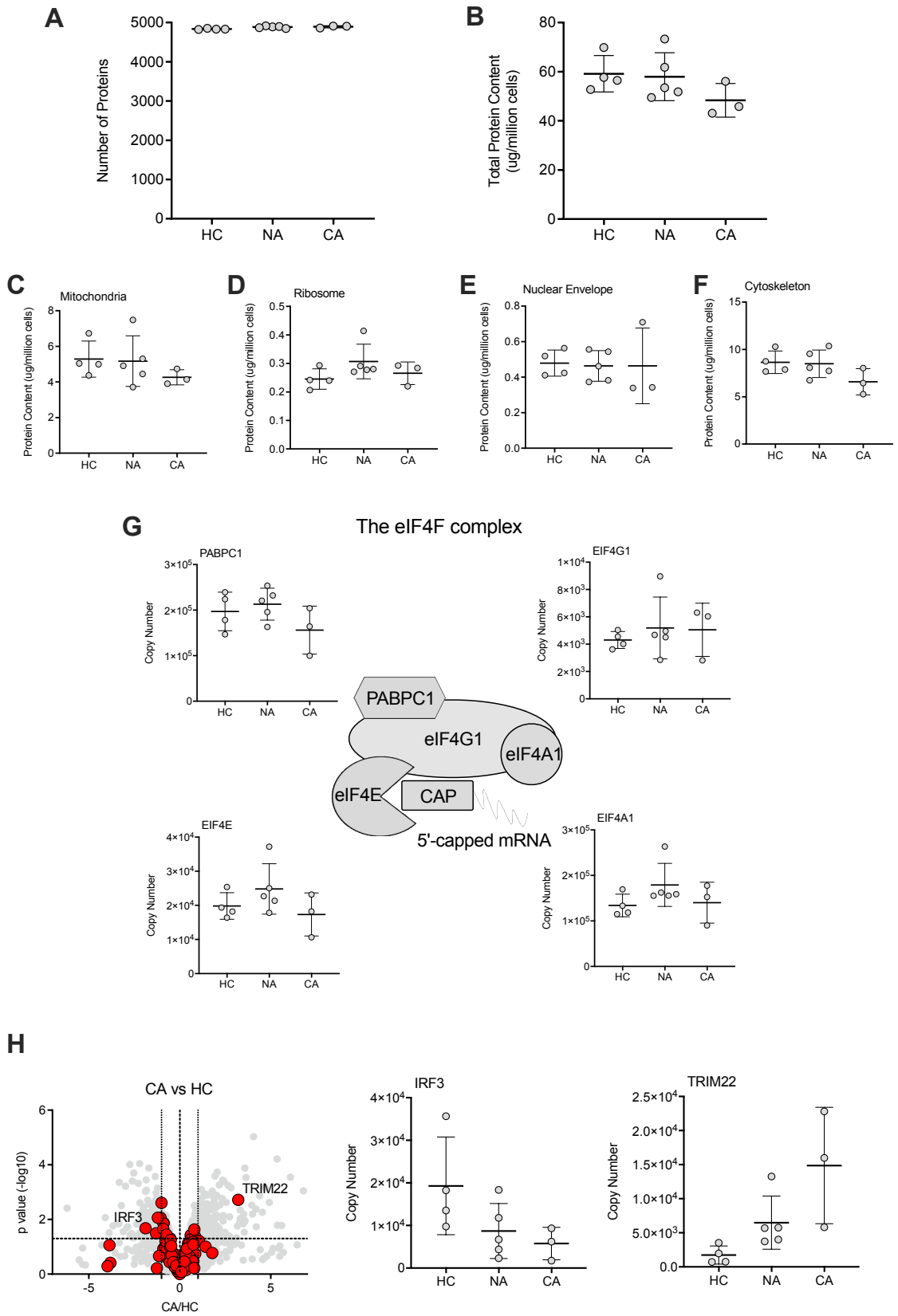

Figure 2. Circulating neutrophils preserve global cellular processes in both COVID-19 and non-COVID-19 ARDS. (A) Number of proteins identified in normal density neutrophils

(NDN) isolated from healthy controls (HC), non-COVID-19 ARDS patients (NA) and COVID-19 ARDS patients (CA). (B-F) Total protein content of NDN, protein content of mitochondria (GO:0005739), ribosomes (Kyoto Encyclopaedia of Genes and Genomes annotation 03010), nuclear envelope (GO:0005635) and cytoskeleton (GO:0001894 and GO:0003008) from the patient cohorts described above. (G) Abundance of components of the eIF4F translation initiation complex (figure adapted from Howden et al., 2019) from the same patient cohorts. (H) Expression profile of transcription factors in CA patients versus HC. Proteins were included with the annotation GO:0003700 (DNA binding transcription factor activity). Horizontal dashed line indicates a P value = 0.05, outer vertical dashed lines indicate a fold change = 2. P values calculated using LIMMA. (A-H) HC (n = 4), NA (n = 5), and CA (n = 3) with data as median ± I.Q.R.

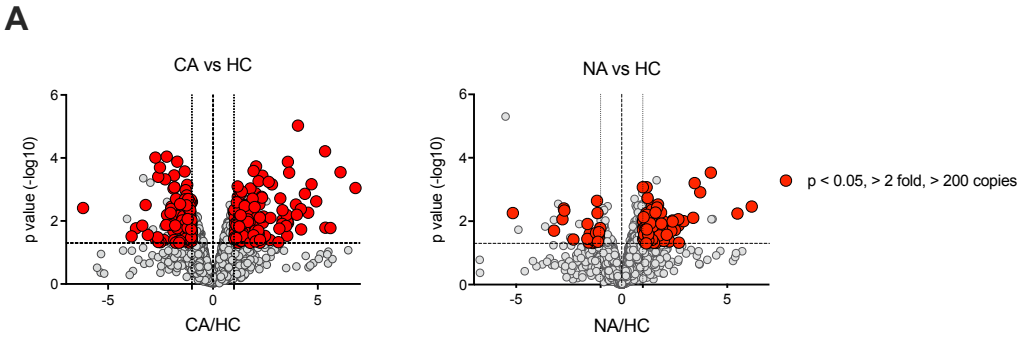

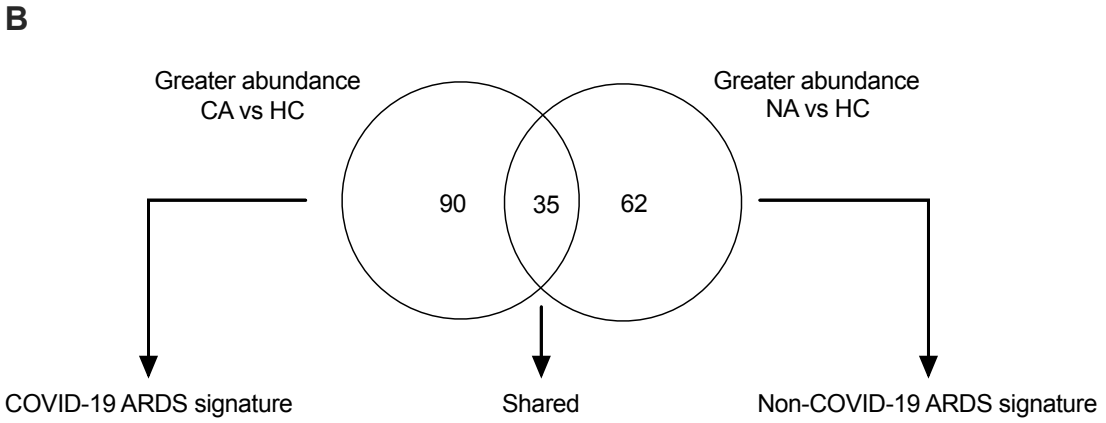

GO:0060337~type I interferon signalling pathway

ID	Gene Name
Q9Y6K5	2'-5'-oligoadenylate synthetase 3(OAS3)
Q15646	2'-5'-oligoadenylate synthetase like(OASL)
P05161	ISG15 ubiquitin-like modifier(ISG15)
Q9Y3Z3	SAM and HD domain containing deoxynucleoside triphosphate triphosphohydrolase 1(SAMHD1)
P23497	SP100 nuclear antigen(SP100)
Q6GPH4	XIAP associated factor 1(XAF1)
P01889	major histocompatibility complex, class I, B(HLA-B)
Q8WXG1	radical S-adenosyl methionine domain containing 2(RSAD2)

GO:0002576~platelet degranulation

ID	Gene Name
P02671	fibrinogen alpha chain(FGA)
P02675	fibrinogen beta chain(FGB)
P02679	fibrinogen gamma chain(FGG)
Q08380	galectin 3 binding protein(LGALS3BP)
P16109	selectin P(SELP)
P01011	serpin family A member 3(SERPINA3)
P05155	serpin family G member 1(SERPING1)
P07996	thrombospondin 1(THBS1)

GO:0006955~immune response

ID	Gene Name
P32246	C-C motif chemokine receptor 1(CCR1)
O76096	cystatin F(CST7)
P27930	interleukin 1 receptor type 2(IL1R2)
Q13478	interleukin 18 receptor 1(IL18R1)
P31785	interleukin 2 receptor subunit gamma(IL2RG)
Q8IYM9	tripartite motif containing 22(TRIM22)

GO:0006821~chloride transport

ID	Gene Name
Q9Y696	chloride intracellular channel 4(CLIC4)
P54105	chloride nucleotide-sensitive channel 1A(CLNS1A)
P02730	solute carrier family 4 member 1(SLC4A1)

GO:0015701~bicarbonate transport

ID	Gene Name
P69905	hemoglobin subunit alpha 1(HBA1)
P68871	hemoglobin subunit beta(HBB)
P02730	solute carrier family 4 member 1(SLC4A1)

Figure 3. Proteome specific remodelling in circulating neutrophils in response to COVID-19 ARDS and ARDS. (A) Proteins showing a significant change in abundance were identified using LIMMA analysis. Proteins were considered to change significantly with a P value <0.05, fold change >2 and a copy number >200 in at least one condition. (B) GO term enrichment analysis for proteins significantly increased in abundance in COVID-19 ARDS (CA) patients and non-COVID-19 ARDS (NA) patients versus healthy controls (HC). Venn diagram shows

the numbers of proteins uniquely increased in abundance in CA and NA and also the number of proteins shared between these 2 groups.

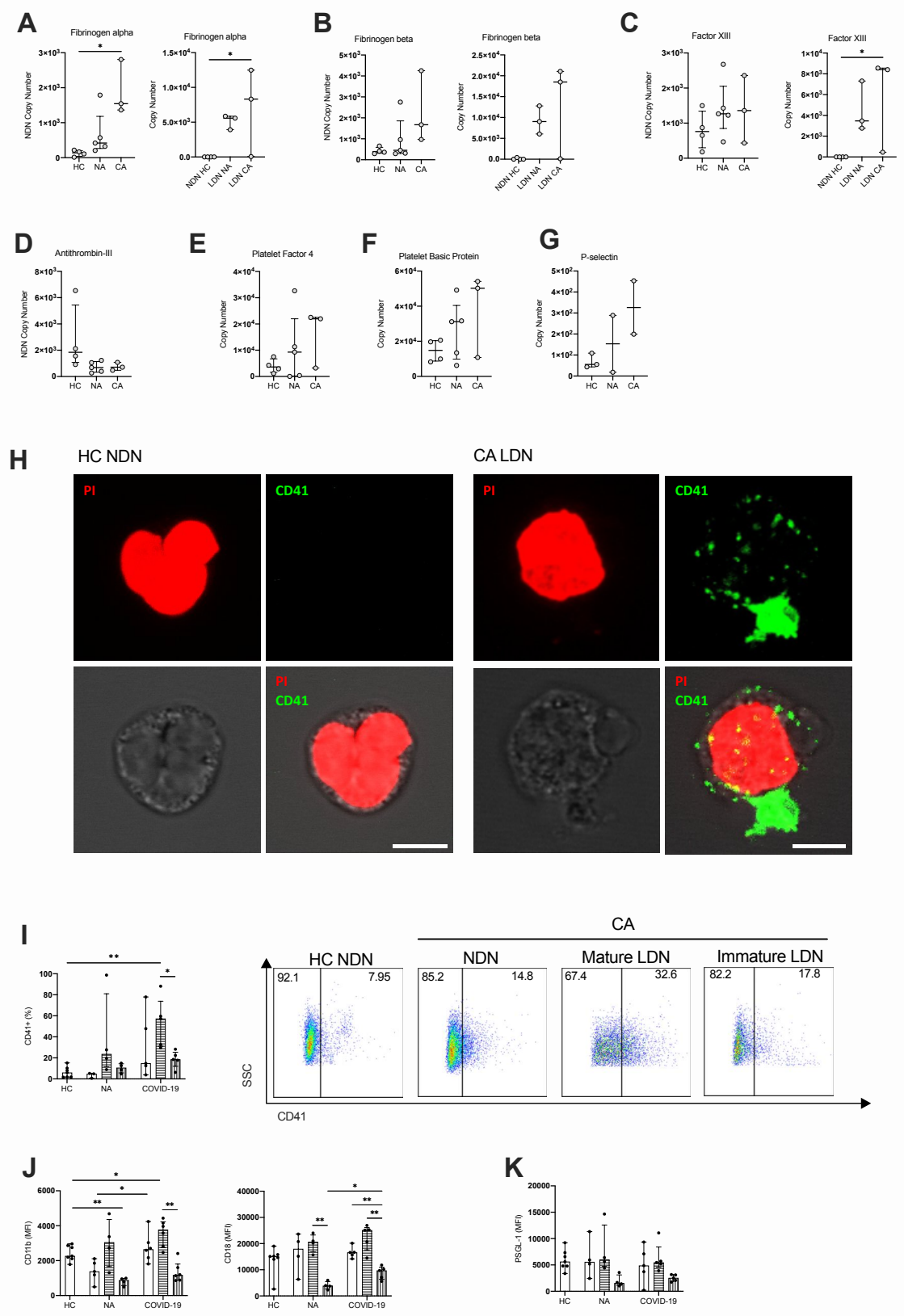

Figure 4. COVID-19 ARDS neutrophils form aggregates with platelets and activate prothrombotic pathways with enrichment in the low-density population. (A-C) Copy

numbers of proteins associated with fibrin clot formation in normal density neutrophils (NDN) isolated from healthy controls (HC), non-COVID-19 ARDS (NA), and COVID-19 ARDS (CA) patients and low density neutrophils (LDN) isolated from NA and CA patients. *$p < 0.05$, determined by Kruskal-Wallis and Dunn's post hoc-testing. (D) Copy number of antithrombin-III in NDN isolated from patient cohorts described above. (E-G) Copy numbers of proteins associated with platelets in NDN isolated from patient cohorts described above. (A-G) NDN from HC (n = 4), NA (n = 5) and CA (n = 3) and LDN (n = 3) with data as median ± I.Q.R. (H) Representative confocal images from NDN obtained from a healthy donor and LDN from a CA patient isolated by FACS and stained for propidium iodide (top left panel, red) and CD41 (top right panel, green). Bright field image was used to delimit cell contour (bottom left panel, grey scale). A composite image is shown in bottom right panel. Scale bar corresponds to 5 μm, 63x magnification. (I) Left, percentage of NDN (open bars), mature LDN (horizontal striped bars) and immature LDN (vertical striped bars) isolated from HC (n = 7), NA (n = 4) or COVID-19 patients (n = 6) with surface expression of CD41. Right, healthy donor and CA representative CD41 dot plots with gate set according to fluorescence minus one control. Data are mean ± SD. *$p < 0.05$, determined by repeated measures two-way ANOVA and Sidak's post hoc-testing; **$p < 0.01$ vs. HC, determined be one-way ANOVA and Holm-Sidak's post hoc-testing. (J) Surface expression of CD11b and CD18 (Mac-1 complex) displayed as geometric mean fluorescence intensity (MFI) determined by flow cytometry analysis of neutrophil populations as described above. Data are mean ± SD. *$p < 0.05$, **$p < 0.01$, determined by repeated measures two-way ANOVA and Sidak's post hoc-testing; *$p < 0.05$, **$p < 0.01$ vs. HC, determined be one-way ANOVA and Holm-Sidak's post hoc-testing. (K) Surface expression of PSGL-1 displayed as MFI determined by flow cytometry analysis of neutrophil populations as described above. Data are mean ± SD.

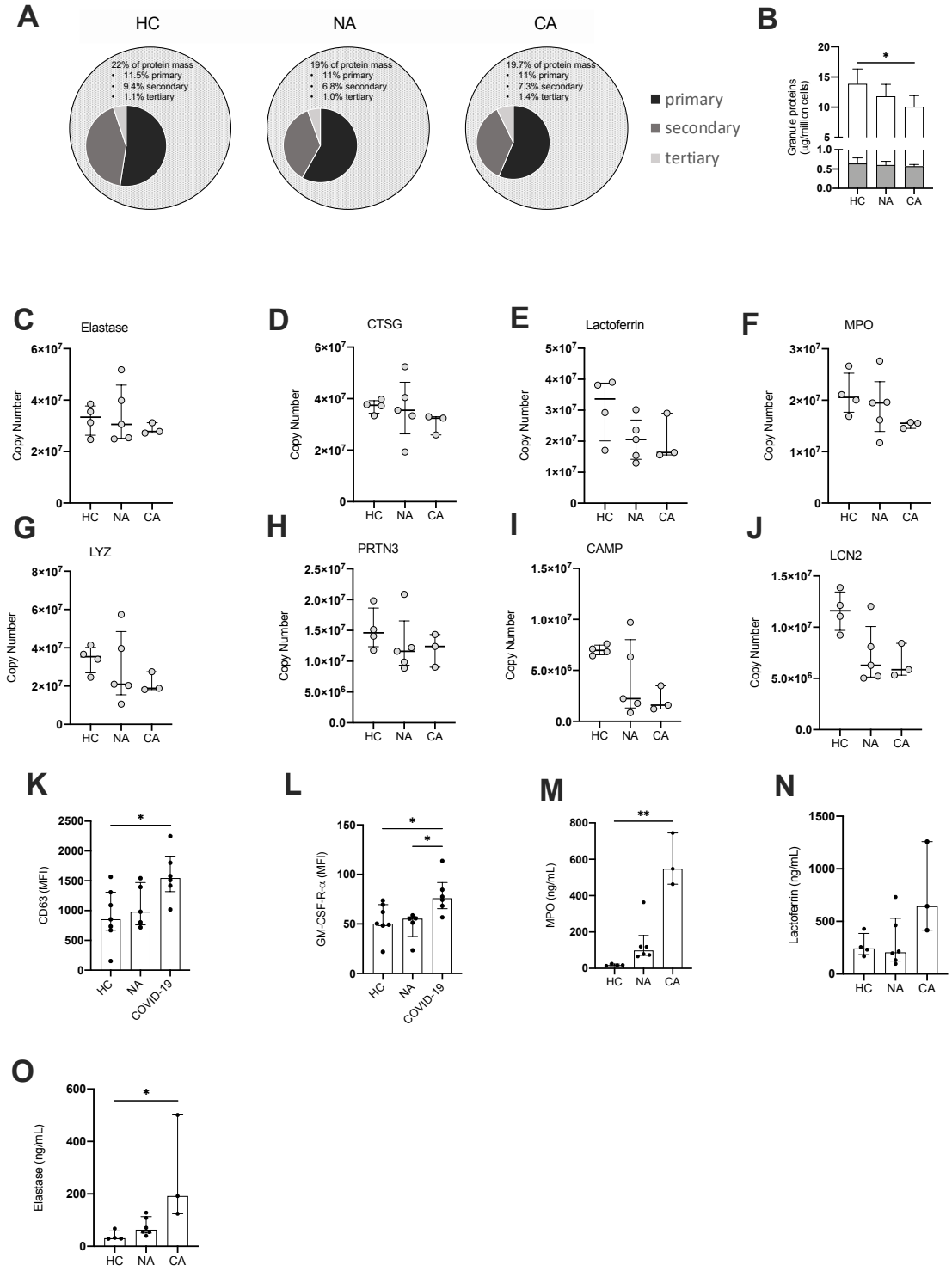

Figure 5. Enhanced circulating neutrophil degranulation in COVID-19. (A) Pie charts show distribution of protein mass in healthy control (HC, n =4), non-COVID-19 ARDS (NA,

n = 5) and COVID-19 ARDS (CA, n = 3) patients. (B) Membrane (grey bars) and content (white bars) granule cargo protein abundance in normal density neutrophils (NDN) isolated from patient cohorts described above. Data are median ± I.Q.R. *$p < 0.05$, determined by Kruskal-Wallis and Dunn's post hoc-testing. (C-J) Copy numbers of granule proteins in NDN isolated from patient cohorts described above. Data are median ± I.Q.R. (K-L) Surface expression of CD63 and GM-CSF-R-α displayed as geometric mean fluorescence intensity (MFI) determined by flow cytometry analysis of NDN isolated from healthy control (n = 7), non-COVID-19 ARDS (n = 5) and COVID-19 (n = 6) patients. Data are median ± I.Q.R. *$p < 0.05$, determined by Kruskal-Wallis and Dunn's post hoc-testing. (M-O) Granule protein levels in serum of HC (n = 4), NA (n = 6), and CA (n = 3) patients measured by ELISA. Data are median ± I.Q.R. *$p < 0.05$, determined by Kruskal-Wallis and Dunn's post hoc-testing.

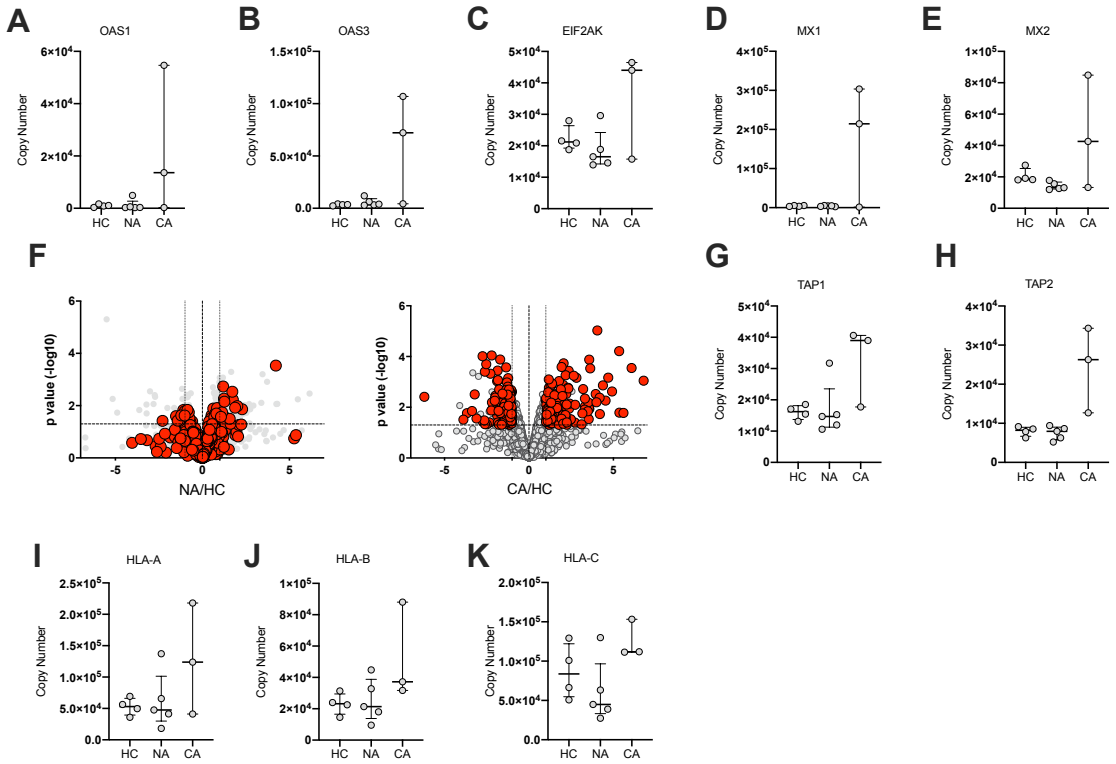

Figure 6. Activation of neutrophil type I interferon signalling pathways and antigen presentation in COVID-19. (A-E) Copy numbers of proteins involved in type I IFN signalling and anti-viral responses in normal density neutrophils (NDN) isolated from healthy controls (HC), non-COVID-19 ARDS (NA) and COVID-19 ARDS (CA). Data are median ± I.Q.R (HC, n = 4; NA, n = 5; CA, n = 3). (F) Expression profile of proteins implicated in development and function of immune cells including antigen processing and presentation and immune cell activation (GO:0002376). (G-H) Copy numbers of TAP proteins in NDN isolated from patient cohorts described above. Data are median ± I.Q.R. (I-K) Copy numbers of MHC molecules in NDN isolated from patient cohorts described above. Data are median ± I.Q.R.

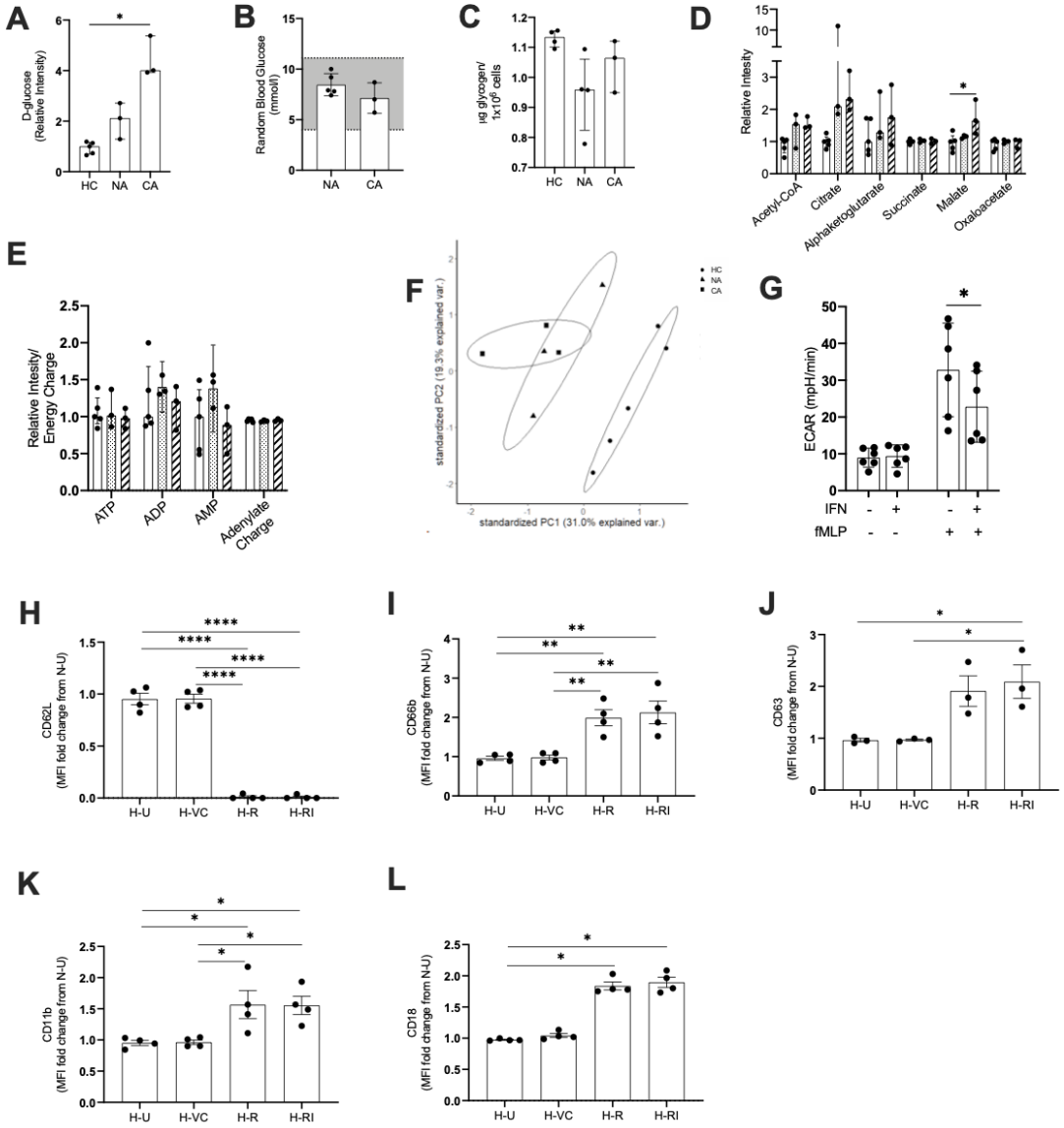

Figure 7. Metabolic rewiring of COVID-19 ARDS neutrophils and changes in neutrophil metabolism in response to type I interferon. (A) D-glucose in normal density neutrophils (NDN) isolated from non-COVID-19 ARDS (NA) and COVID-19 ARDS (CA) expressed relative to NDN isolated from healthy control (HC) was identified by metabolic analysis. Data are median ± I.Q.R (HC, n = 5; NA, n = 3; CA, n = 2). *$p < 0.05$, determined by Kruskal-Wallis and Dunn's post hoc-testing. (B) Random blood glucose measurements were obtained from NA and CA patients on the day of sampling with dotted horizontal lines representing upper and lower limits for random blood glucose in individuals without diabetes mellitus. Data

are mean ± SD (NA, n = 5; CA, n = 3). (C) Glycogen content in NDN isolated from patient cohorts as described in (A) was measured using a fluorometric assay. Data are median ± I.Q.R. (D) Targeted metabolites in NDN isolated from HC (white bars), NA (spotted bars) and CA patients (diagonal striped bars) were identified by metabolic analysis. For each metabolite, relative intensity was calculated by normalising each data point to the mean of the HC population. Each data point represents mean of duplicate samples and summarised as median ± I.Q.R. (HC, n=5; NA, n=3; CA, n=3). *$p < 0.05$, determined by Kruskal-Wallis and Dunn's post hoc-testing. (E) Targeted metabolites in NDN isolated from patient cohorts as described in (D) were identified by metabolic analysis and adenylate charge calculated. (F) Principle component analysis (PCA) of target metabolites for patient cohorts described above and indicated by shapes. (G) Glycolytic reserve as observed by extracellular flux analysis using the glycolysis stress test in healthy control NDN with IFNα/ IFNβ (+) or control (-) for 4 h and stimulated (+) with fMLP immediately prior to analysis. Data are mean ± SD (n = 6, individual data points represent mean of at least two technical replicates from individual donors). *$p < 0.05$, determined by repeated measures two-way ANOVA and Tukey's post hoc-testing. (H-L) Surface expression of neutrophil activation markers expressed as a fold change of geometric mean fluorescence intensity (MFI) from HC NDN under untreated normoxic conditions (N-U) as determined by flow cytometry analysis of healthy control NDN cultured in hypoxia under untreated conditions (H-U), with resiquimod (H-R) or in combination with IFNα/ IFNβ (H-RI) for 1 hour. HC NDN cultured with vehicle control (H-VC) also included. Data are mean ± SD (n = 3-4). *$p < 0.05$, **$p < 0.01$, ****$p < 0.0001$ determined by one-way ANOVA and Holm-Sidak's post hoc-testing.